Reliability of Thermal Images and Numerical Modelling on Passive Infrared Thermography for Concrete Structures

Kavya R. Nair [1a], Vimal Mohan [2], P. Srinivasan [2]

[1] Project Associate, CSIR- Structural Engineering Research Centre, Taramani, Chennai
[1] Scientist, CSIR-Structural Engineering Research Centre, Taramani, Chennai
[a]*Email: krn.kavyanair@gmail.com*

Abstract

Premature deterioration of reinforced concrete (RC) structures resulting from exposure to aggressive environments is a serious challenge faced by civil engineers. Highway bridges, marine structures, and industrial power plants are typical examples of structures facing premature deterioration. Evaluation of concrete quality and deterioration in concrete structural elements using non-destructive testing methods such as Infrared Thermography (IRT) plays a vital role. Defects such as honeycombs, delamination etc can be identified based on the temperature variation on the thermograms. But, the depth of delamination cannot be determined. In this paper, experimental studies were carried with different depths of delamination & numerical studies based on heat transfer were performed. The depth of delamination obtained from the numerical model was found to be matching with the experimental studies and the numerical model was validated.

Keywords: *Concrete deterioration, Non-destructive testing, Infrared thermography, Numerical modelling, Defect quantification*

1. Introduction

Concrete is one of the most versatile man-made building materials available. But due to various factors like extreme weather condition, improper construction methods, corrosion etc. premature deterioration occurs in concrete structures [1]. These deteriorations in the form of cracks, delaminations and air voids, which will start slowly will progress to failure and can be expensive in terms of money and life. The ability to detect these deteriorations at early stage itself act as a useful tool for maintenance and restoration of structure. The methods include Non-destructive tests (NDT) which cause no damage to the structure and also methods like core test, pull out test etc. which affects the integrity of the structure and require repair after the test. With the advances in image processing, signal processing and increased access to powerful computers NDT has become a powerful tool for the analysis of old as well as new concrete structures (Hiasa, 2014). Currently various methods like impact echo, coin tapping, ultrasonic pulse echo, ultrasonic surface wave, ground penetrating radar and infrared thermography are applied for defect detection in concrete [2].

Infrared thermography (IRT) is a global inspection method which allows to detect subsurface delaminations and voids with accuracy. It is having the advantage of inspecting large surface area without direct contact in a short span of time which make it useful for application in wide range of civil engineering structures [3]. Infrared thermography is the science of detecting infrared energy emitted from an object, converting it into apparent temperature and displaying the result as an infrared image. Using an infrared camera, the thermal image can be obtained from an object without making direct contact with the object and this makes IRT an ideal method for investigating inaccessible structures [4].

All objects above zero Kelvin emit infrared energy. IR camera detects this IR energy and convert that to temperature and gives thermogram as output. Heat flows from warmer to cooler area and sound concrete have least resistance to heat conduction. Presence of defects/deteriorations reduces the conductivity as it is having thermal conductivity less than concrete. Thus, the portion of concrete above the defect will be having higher temperature than surrounding during day time (Fig.1 a) and during night that portion will be cold (Fig.1 b). This variation in temperature can be identified from thermogram indicating defects [5].

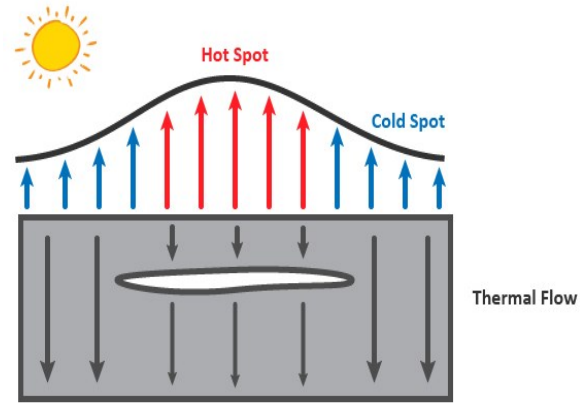

(a)

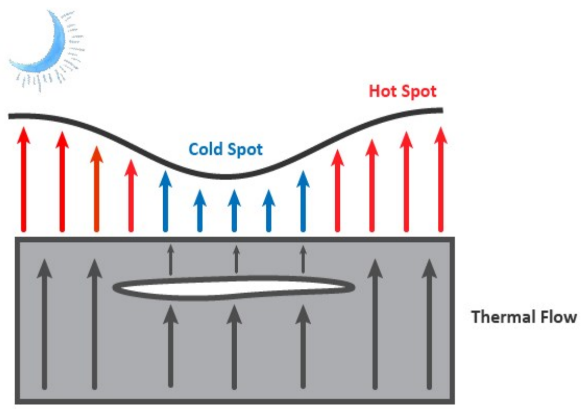

(b)

Fig.1: (a) Temperature variation during day time (b) during night

Concrete testing can involve large areas, the heat source should be low cost and capable of heating the surface uniformly. Sun fulfils all these requirements and this method is called passive infrared thermography. For areas not accessible to sunlight an external source of heat is to be provided and this method is called active thermography. Since concrete is having low thermal diffusivity it requires long heating time which is practically not possible with active IRT. Also, concrete is highly non-homogenous which means that the use of active IRT is less widely reported in civil engineering than in other fields [6]. Estimating the depth of delamination is a major limitation of IRT. Quang Huy Tran et.al [7] conducted study using square pulse thermography which is a method of active IRT for defect quantification. A relation between observation time and square of real depth was derived to find the depth of defect. Also, a method for evaluation of depth and thickness of defect based maximum thermal contrast, defect size, sample thickness and heating time under active IRT was suggested. But for passive thermography these methods cannot be used.

This study aims at conducting an experimental investigation on concrete specimens with defects of thickness 3 mm and 10 mm kept at various depths from surface. Passive infrared thermography is utilized for defect detection. The variation in temperature of delaminated area with depth of defect, thickness and time of investigation is studied in detail. Also, this study investigates the possibility to estimate the depth of defect using FE modelling.

2. Experimental Program

2.1 Specimen details

In this study four specimens with defects simulated with different thickness and depth were used. Details about the dimension of specimen and depth and type of defects in each is given in Table I. Fig.2 shows the details about the specimen and arrangement of defects. Artificial delamination was simulated using Expanded Polyethylene (EPE) foam and cardboard and one with air gap. EPE foam was chosen because it is having a thermal conductivity of 0.024 W/m K which is similar to that of air and cardboard is having lot of air voids in it which simulate the condition similar to an air void/delamination. For SA-1 an air gap was created at one edge of the specimen to study the effect of boundary condition on defect detection. A steel plate was placed at a depth of 20 mm during casting and was removed after four hours leaving an air gap inside. Concrete of M30 grade was used for the preparation of specimens.

Table.I: Statistical Parameters of UPV Values

Specimen	Size of specimen (mm)	Defect type	Size of defect(mm)	Defect depth (mm)
SA-1	500 x 500 x 125	Air void	165 x 165 x 3	20
S-1	500 x 500 x 150	Card board EPE foam	100 x 100 x 3 100 x 100 x 10	12
S-2	500 x 500 x 150	Card board EPE foam	100 x 100 x 3 100 x 100 x 10	25
S-3	500 x 500 x 100	Card board EPE foam	100 x 100 x 3 100 x 100 x 10	30 & 40

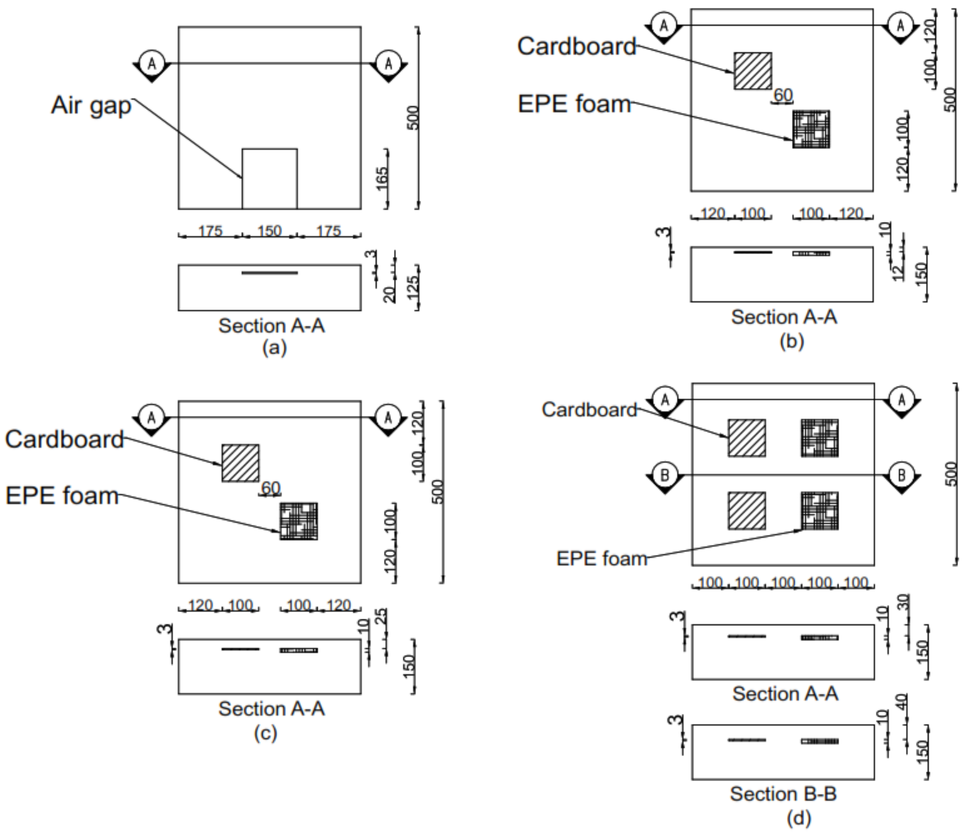

Fig.2: (a) Specimen 1(SA-1) (b) Specimen 2(S-1) (c) Specimen 3(S-2) (d) Specimen 4 (S-3)

2.2 Test procedure

Specimens were arranged on an open ground over concrete cubes of 100 mm size to ensure wind flow for proper heat transfer. Infrared images were taken using IR camera from 9 AM to 6 PM at one-hour interval. The emissivity value was set as 0.95 which is the value for concrete and the reflected apparent temperature was set as 6°C. Slabs were arranged in north- south direction and images were taken from a height of 1.5 m from concrete surface. Specifications of camera is given is Table II.

Table II: IR Camera specifications

Detector type	Uncooled microbolometer
IR resolution	320 x 240 pixels
Spectral range	7.5 - 13 µm
Field of view	45^{O} x 34^{O}

3. Experimental Output

3.1 IR output for SA-1

In the image from 9 AM, the defect was partially detected and then as time passes it became more visible upto 12 PM. After 12PM the edge with air gap was having less temperature as the sun shifts to opposite side and the air gap was not detected. At 2 PM the defect was only partially detected and after that is was not visible. Table III summarizes the IRT results for SA-1. Also, in terms of difference in temperature between sound and delaminated portion (ΔT) it was found that during 10 AM to 1 PM even with ΔT of 1.4°C the defect was detected were as at 9 AM and 6 PM even with ΔT of 2 °C and 2.6 °C defects was not detected. Thus, it can be inferred that the delamination being near to the boundary is having an effect on defect detectability. But this will not be a problem for actual structures which have larger surface area. Fig. 3 shows the IR images for SA-1 at 9 AM, 1 PM and 4 PM.

Table III: Summary of IRT results

Time	**9 AM**	**10 AM**	**11 AM**	**12 PM**	**1 PM**	**2 PM**	**3 PM**	**4 PM**	**5 PM**	**6 PM**
Sun loading	C	C	C	C	C	C	C	C	O	O
Defect indication	P	C	C	C	C	P	O	O	O	O
Heating/ cooling	Hg	Hg	Hg	Hg	Hg	Cg	Cg	Cg	Cg	Cg

Indications: C- defect completely detected, P- defect partially detected, O- defect not detected, Hg- Heating
Cg- Cooling

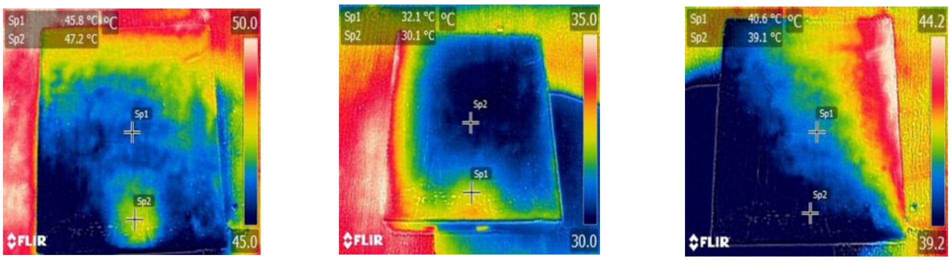

Fig. 3: IR images for SA-1

3.2 IR output for S-1 to S-3

From IR images it was observed that the defect detectability is affected by the thickness of the defect and depth of defect. For specimen 1 in which defect is at 12 mm depth both the defects were completely detected from 10 AM to 2 PM and during 6 PM. During 9 AM, 2 PM and 5 PM defects were only partially detected. This is because of the interchange of heating and cooling cycle. And it was observed that during 4 PM defects were not detected, and this is because of the intersection of heating and cooling cycle. This was found to be true for all the specimens. For specimen 2 in which defect was at 25 mm depth from surface 3mm thick defects were not detected at any instant of time. For 10 mm defect also, it was only partially detected from 10 AM to 3PM. Table IV summarizes the IRT results for S-1 and S2 respectively. A defect like portion is seen on the left top corner for specimen-2 in all the images. But this was identified as a stain mark on the top of the specimen from digital image.

From the IR images for specimen 3 it was observed that the defects; both 3 mm and 10 mm was not detected at any time. Some portions similar to defects was identified. But the temperature for that portion is less than sound region which is not true for day time heating condition. It was found from digital image that such observations are due to the smooth finish of the surface. Fig.4-6 shows the IR images obtained for three specimens.

Table IV: Summary of IRT results for S1 and S2

Time	9AM	10AM	11AM	12PM	1PM	2PM	3PM	4 PM	5 PM	6 PM
Sun loading	C	C	C	C	C	C	C	C	O	O
Defect indication S-1 (10mm)	C	C	C	C	C	C	P	O	P	C
Defect indication S-1 (3mm)	P	C	C	C	C	C	P	O	P	C
Defect indication S-2 (10 mm)	O	P	P	P	C	P	P	O	O	O
Defect indication S-2 (3mm)	O	O	O	O	O	O	O	O	O	O

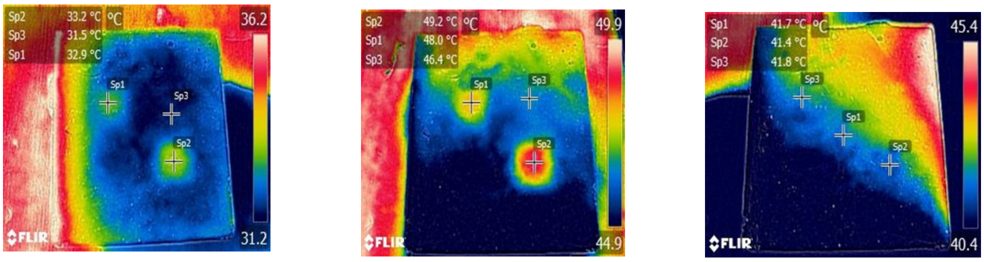

9 AM 1 PM 4 PM

Fig. 4: IR images for S-1

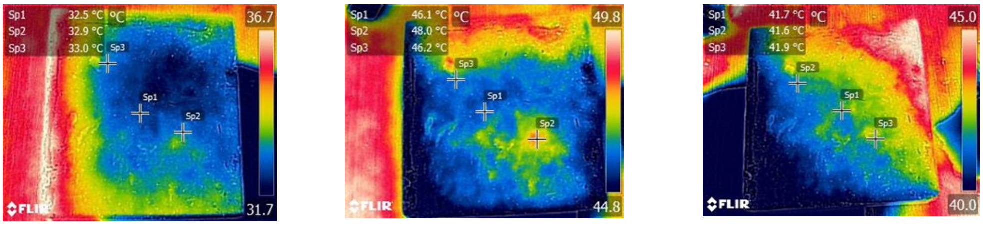

9 AM 1 PM 4 PM

Fig. 5: IR images for S-2

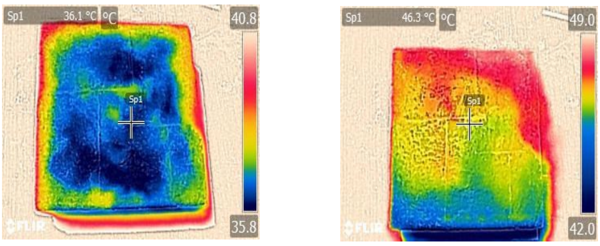

11 AM 12 PM

Fig. 6: IR images for S-3

3.3 Discussion of experimental outputs

From experimental investigation it was found that defects up to 25 mm depth could be detected. Also, at 25 mm depth only delamination with 10 mm thickness could be detected. At 4 PM, defects were not detected in any of the specimens. This is due to the intersection of heating and cooling cycle. Also, for specimen SA-1 defect were not detected after 3PM. This is due to the boundary condition and interchanging period. It was observed that the surface temperature of delamination (T_{del}) was higher than temperature of sound area (T_{sound}) during heating cycle. And during cooling cycle T_{del} is less than T_{sound}. Also, it was observed that the T_{del} value decreases with increase in depth of defect. Fig. 7 shows the variation of T_{sound} and T_{del} with time. It was observed that T_{del} value varies with the thickness of defect. T_{del} value was more for 10 mm thick defects during heating cycle and T_{del} for 3mm thick defect more than that for 10 mm defects during cooling cycle. Fig.8 shows the variation of T_{del} with thickness of defect. Thus, a correlation between the depth of defect and thickness of defect with T_{del} is obtained such that T_{del} decreases with increase in depth and increases with increase in thickness.

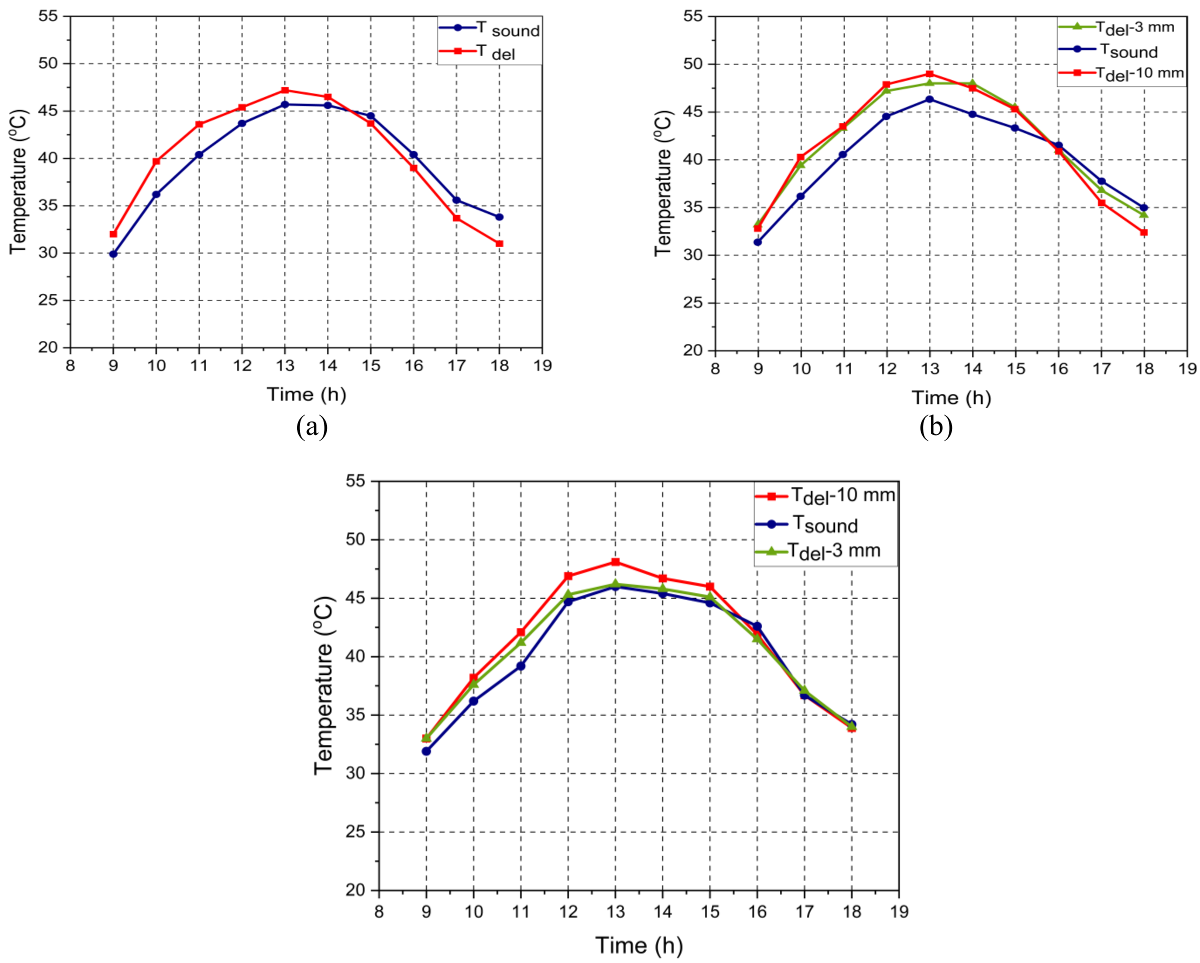

(a) (b)

(c)

Fig.7: Variation of T_{sound} and T_{del} with time. (a)SA-1 (b)S-1 (c)S-2

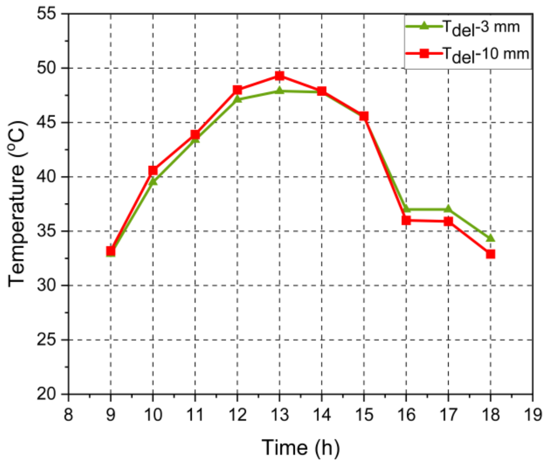

(a)

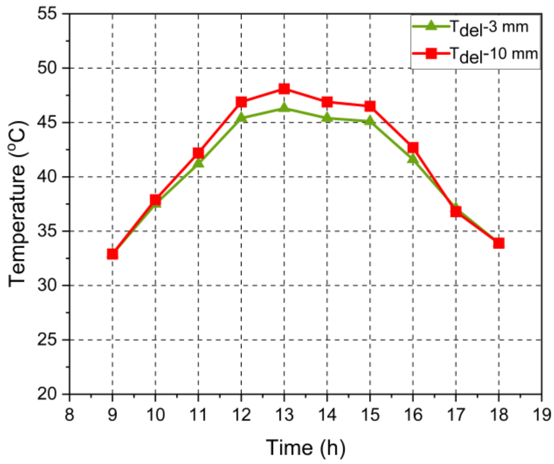

(b)

Fig. 8: Variation of T_{del} with thickness of defect(a) S-1 (b)S-2

4. Numerical Model

4.1 Model development

Finite element modelling of the specimens was done and results were compared with IRT results to validate the model. Modelling was done using the Heat transfer module of COMSOL Multiphysics software.

The concrete blocks of size 500 mm x 500 mm x 150 mm were established over a large ground of size 6 x 6 x 1 m. Defects in form of EPE foam was arranged similar to specimen at depth of 12mm, 20mm, 25 mm. The blocks were arranged over concrete stand of width 100 mm and height 150 mm.

Fig.9(a)shows the FE model of the specimen along with ground. Meshing of the model was done using "Finer" element size physics-controlled mesh available in the software. The material properties fed are given in Table V. The parameters like solar irradiance, ambient temperature, convective heat transfer coefficient, location information and date of experimental investigation are required for forming the FE model. The solar irradiance I_s=605 W/m^2 was set in software for all the models. The ambient temperature input was given based on the weather condition reported by the nearest weather station. The ambient temperature value given as input is given in Fig.9(b).

In this model the primary heat source is the solar radiation. The value of solar radiation and direction of sunlight with time was automatically calculated by the software using latitude, longitude, time zone, date and time. The information was fed as follows: latitude=13.083, longitude=80.2707, time zone= +5:30 h. Convective heat transfer co-efficient h_w was calculated using wind speed. The average value of wind speed for the day was found to be 5.04 m/s. And h_w was obtained as 23 W/ m^{2}K.

Table V: Material properties

Material properties	**Units**	**Concrete**	**EPE foam**	**Ground**
Thermal conductivity	W/ (m K)	1.6	0.024	0.6
Heat capacity at constant pressure	J/ (kg K)	880	1130	800
Density	Kg/m^3	2300	25	1500
Surface emissivity	-	0.95	-	0.76

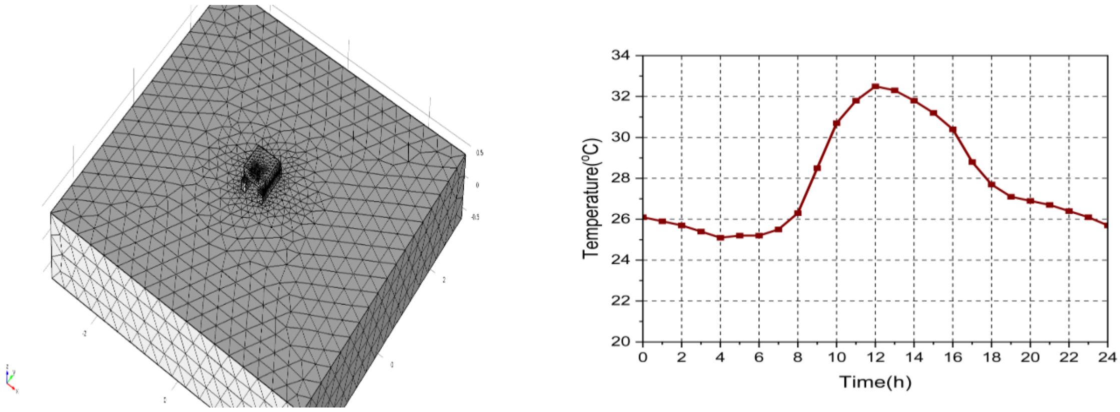

Fig.9: (a)FE model of specimen along with ground (b)Ambient temperature for 4th March 2022

5. Comparison of Simulation and IR Results

Simulation results were obtained from 9 AM to 6 PM. Fig.10-12 shows the simulation results for 9 AM, 1 PM and 4 PM. The defects are clearly visible in simulation results similar to IR results. At 4 PM the simulation result also shows the interchange period during which the defects were not visible in the image. Fig. 7 shows the comparison between IR results and simulation results. The simulation results also follow a similar pattern with experimental values. Surface temperature values from 12 PM to 3 PM is almost same for both simulation and experimental results for S-1 and S-2 (Fig.13). And it is same at 2PM for SA-1. This exceptional behaviour of SA-1 is due to the boundary condition. During other times of the day the temperature readings are bit higher for simulation results. This might be because of the assumption that the sky was clear entire day which was made while doing FE modelling.

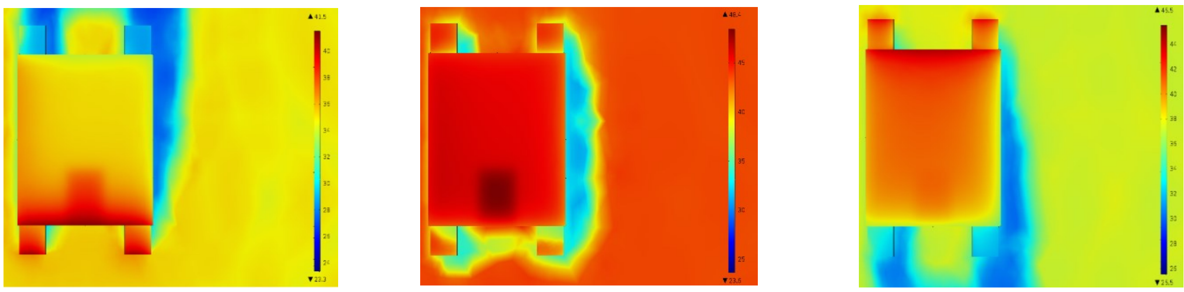

9 AM 1 PM 4 PM

Fig.10: Simulation result for SA-1

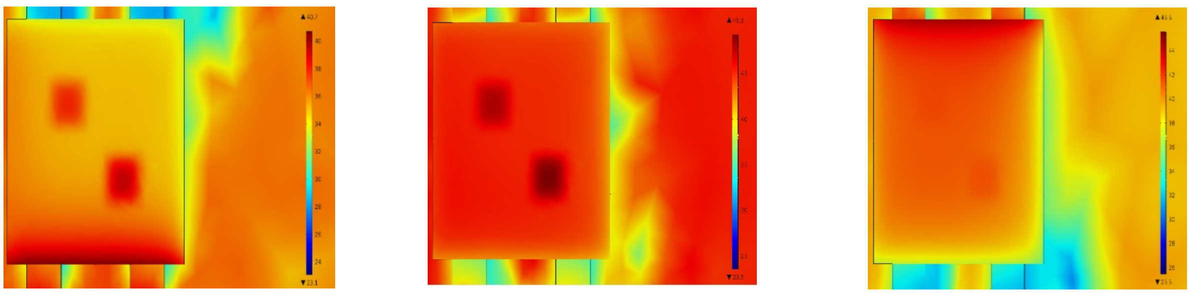

9 AM 1 PM 4 PM

Fig.11: Simulation results for S-1

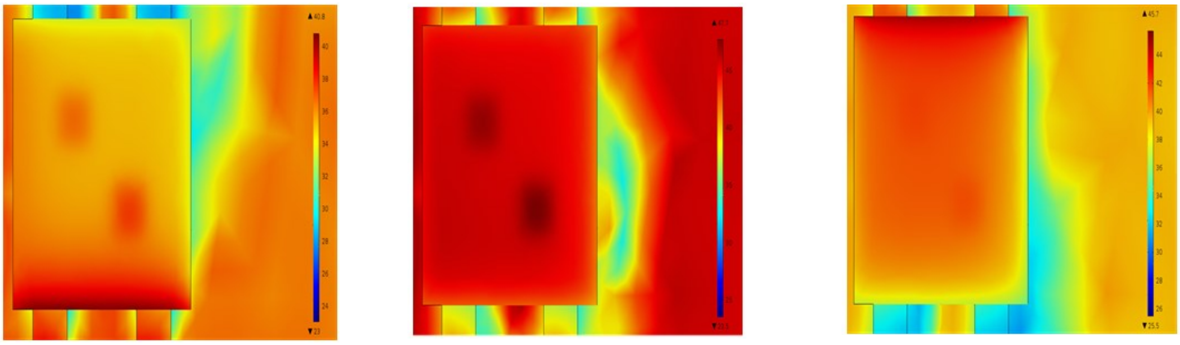

9 AM 1 PM 4 PM

Fig.12: Simulation results for S-2

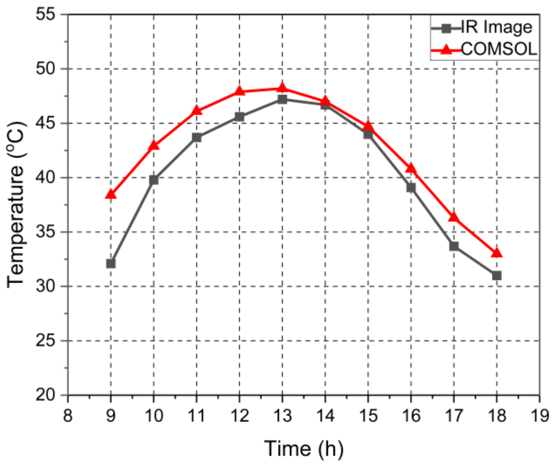

(a)

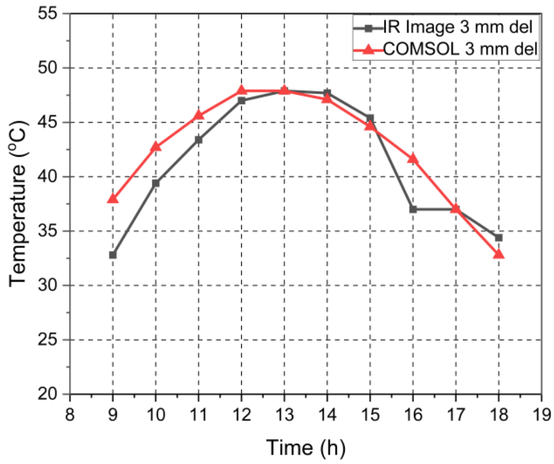

(b)

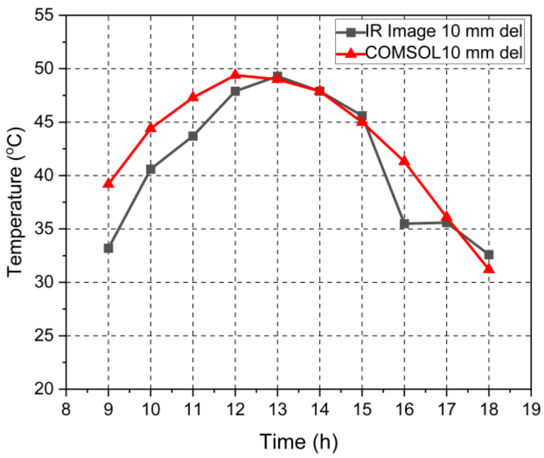

(c)

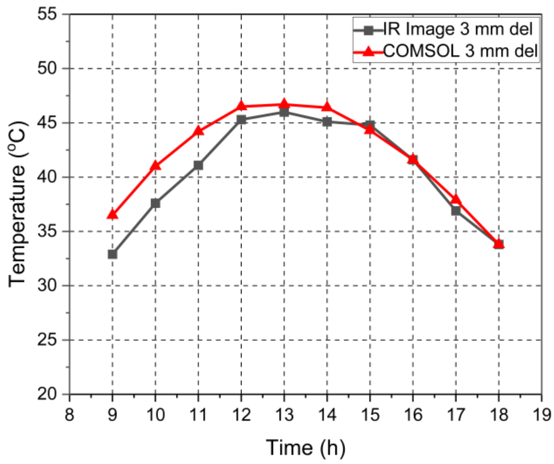

(d)

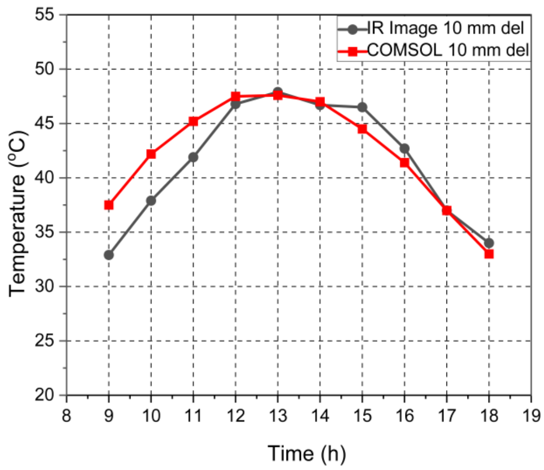

(e)

Fig.13: Comparison of simulation result and IR result (a)SA- 1 (b)S-1, defect 3mm thick (c)S-1, defect 10 mm thick (d) S-2, defect 3mm thick (e)S-2, defect 10 mm thick

From the comparison of simulation and IRT results it can be concluded that the FE model was established properly. A similar pattern of T_{del} values was obtained from simulation results. The values of temperature were almost same during 12 PM to 3 PM. But it can be found that during other time the values of temperature was higher than the IR results. This can be due to the assumption of clear sky condition made while creating FE model. The other reasons include some external agents like wind, photographic angle, thermal sensitivity of camera etc. Thus, it can be concluded that an inverse study can be conducted using FE modelling by simulating several depths and thicknesses of delamination models from which the depth of delamination can be obtained.

6. Conclusion

Experimental investigation was done on specimens with simulated defects to study the effectiveness of IR thermography for detecting delaminations in concrete structures. It was found that IRT can be used effectively for evaluating quality of cover concrete. Defects upto a depth of 25mm can be detected from IR images. An interchange period between heating and cooling cycle was observed and during which the defects are not detected in IR images. From SA-1 it was found that the boundary condition is having much effect on the defect detectability and temperature values. But this will not be a problem for actual structures which have larger surface area. Sometimes the portion identified as defect from the image can be some stains or marking on the surface of the defect. Comparing IR image with digital image helps to overcome this problem. A correlation between the depth of defect and thickness of defect with T_{del} was obtained such as T_{del} increases with increase in thickness of defect and decreases with increase in depth from surface. Numerical model was established successfully using COMSOL Multiphysics software and the temperature values between 12 PM and 3 PM shows a similar trend with IR results. Thus, it could be concluded that an inverse study can be conducted using FE modelling by simulating several depths and thickness of delamination models from which the depth of delamination can be obtained.

7. References

[1] Jungwon Huh, Quang Huy Tran, Jong-Han Lee, DongYeob Han, Jin-Hee Ahn, and Solomon Yim (2016). "Experimental study on detection of deterioration in concrete using infrared thermography technique". Advances in Materials Science and Engineering, https://doi.org/10.1155/2016/1053856.

[2] Shuhei Hiasa, Recep Birgul, Azusa Watase, Masato Matsumoto, Koji Mitani and F. Necati Catbas (2014). "A Review of Field Implementation of Infrared Thermography as a Non-destructive Evaluation Technology". Computing in Civil and Building Engineering ASCE 1715-1722, 10.1061/9780784413616.213.

[3] Shuhei Hiasa, Recep Birgul, F. Necati Catbas (2017). "Effect of Defect Size on Subsurface Defect Detectability and Defect Depth Estimation for Concrete Structures by Infrared Thermography". J Nondestruct Eval 36:57, https://doi.org/10.1007/s10921-017-0435-3

[4] M. Hain, J. Bartl, V. Jacko (2009). "Active Infrared Thermography in Non-destructive Testing". Institute of Measurement Science Slovak Academy of Sciences, Bratislava, Slovak Republic, 5, 339–343, 10.1117/12.881599.

[5] Azusa Watase, Recep Birgul, Shuhei Hiasa, Masato Matsumoto, Koji Mitani, F. Necati Catbas (2015). "Practical identification of favorable time windows for infrared thermography for concrete bridge evaluation". Construction and Building Materials 101 1016–1030, 10.1016/j.conbuildmat.2015.10.156.

[6] Patricia Cotič, DejanKolarič, Violeta Bokan Bosiljkov, Vlatko Bosiljkov, Zvonko Jagličić (2015). "Determination of the applicability and limits of void and delamination detection in concrete structures using infrared thermography". NDT&E International74, 87–93, https://doi.org/10.1016/j.ndteint.2015.05.003.

[7] Tran Q. H, Huh J, Mac V. H, Kang C, & Han D (2018). "Effects of rebars on the detectability of subsurface defects in concrete bridges using square pulse thermography". NDT and E International, 100, 92–100, https://doi.org/10.1016/j.ndteint.2018.09.001.

[8] Shuhei Hiasa, Recep Birgul, F. Necati Catbas (2017). "A data processing methodology for infrared thermography images of concrete bridges". Computers and Structures 190 ,205–218, https://doi.org/10.1016/j.compstruc.2017.05.011.

[9] Jungwon Huh, Quang Huy Tran, Jong-Han Lee, DongYeob Han, Jin-Hee Ahn, and Solomon Yim (2016). "Experimental study on detection of deterioration in concrete using infrared thermography technique". Advances in Materials Science and Engineering, 10.1155/2016/1053856

[10] A. Karunarathne (2016). "Modelling of Thermal Effects due to Solar Radiation on Concrete Pavements". Int. Conf. Int. Inst. Infrastruct. Resil. Reconstr., no. 8, p. 277.

[11] Basic Guide to Thermography (2004), Land Instruments International.

[12] B. Milovanovic (2012). "The Role of Infrared Thermography in Nondestructive Testing of Concrete Structures". vol. 385, no. 1, pp. 7–12.

[13] Glenn Washer, Richard Fenwick, and Naveen Bolleni (2010). "Effects of Solar Loading on Infrared Imaging of Subsurface Features in Concrete". J. Bridge Eng.15:384-390, https://doi.org/10.1061/(ASCE)BE.1943-5592.0000117.

[14] Hiasa S, Birgul R, MatsumotoM & Necati Catbas F (2018). "Experimental and numerical studies for suitable infrared thermography implementation on concrete bridge decks. Measurement". Journal of the International Measurement Confederation, 121(February), 144–159, https://doi.org/10.1016/j.measurement.2018.02.019

[15] Malhotra V.M, Carino N.J. Handbook on Nondestructive Testing of Concrete, 2nd ed.; CRC Press: Boca Raton, FL, USA, 2004.

[16] Shuhei Hiasa, Recep Birgul, Masato Matsumoto and F. Necati Catbas(2018). "Experimental and Numerical Studies for Suitable Infrared Thermography Implementation". https://doi.org/10.1016/j.measurement.2018.02.019.

[17] M. Mirsadeghi, D. Cóstola, B. Blocken, and J. L. M. Hensen (2013) "Review of external convective heat transfer coefficient models in building energy simulation programs: Implementation and uncertainty," Appl. Therm. Eng., vol. 56, no. 1–2, pp. 134–151, https://doi.org/10.1016/j.applthermaleng.2013.03.003